Available online at www.sciencedirect.com

ScienceDirect

Proceedings of the Combustion Institute 36 (2017) 4321–4328

Proceedings of the Combustion Institute

www.elsevier.com/locate/proci

Hetero-/homogeneous combustion of fuel-lean methane/oxygen/nitrogen mixtures over rhodium at pressures up to 12 bar

Ran Sui, John Mantzaras*, Rolf Bombach, Alexey Denisov

Paul Scherrer Institute, Laboratory of Thermal Processes and Combustion, CH-5232 Villigen PSI, Switzerland

Received 1 December 2015; accepted 1 June 2016
Available online 15 June 2016

Abstract

The hetero-/homogeneous combustion of $CH_4/O_2/N_2$ mixtures over rhodium was investigated experimentally and numerically at fuel-lean equivalence ratios $\varphi = 0.30$–0.40, pressures 2–12 bar, and catalyst temperatures 700–1250 K. Experiments were performed in an optically accessible channel-flow reactor coated with rhodium and included in situ Raman measurements of major gas-phase species concentrations across the channel boundary layer for evaluating the catalytic processes, and planar laser induced fluorescence (LIF) of the OH radical for assessing homogeneous combustion. Computations were carried out with a 2-D elliptic code, using detailed heterogeneous and homogeneous chemical reaction mechanisms. Comparisons between Raman-measured and numerically-predicted transverse profiles of the limiting reactant (methane) mole fractions have led to the evaluation of the performance of detailed surface reaction mechanisms and to the construction of a one-step catalytic reaction suitable for pressures up to 12 bar. For the investigated range 2–12 bar, the catalytic reactivity of methane over rhodium exhibited an overall positive pressure dependence $\sim p^{0.30}$, which was weaker compared to an earlier-reported pressure dependence of methane over platinum ($\sim p^{0.47}$). Comparisons of the planar OH-LIF measurements with numerical simulations employing different gas-phase reaction mechanisms demonstrated that the correct prediction of homogeneous ignition was particularly demanding at the present low equivalence ratios and moderate reactor temperatures. An elementary gaseous reaction mechanism was shown to reproduce the measured homogeneous ignition distances at all pressures, particularly when used in conjunction with the herein proposed one-step catalytic reaction.

Keywords: Catalytic combustion of methane at elevated pressures; Rhodium catalyst; Pressure dependence of catalytic reactivity; In situ Raman and LIF measurements; Homogeneous ignition of methane over rhodium

1. Introduction

The complete oxidation of methane over noble metals is of prime interest in many industrial applications encompassing large-scale power plants [1], microreactors for portable power generation [2] and

* Corresponding author. Fax: +41 56 3102199.
E-mail address: ioannis.mantzaras@psi.ch (J. Mantzaras).

http://dx.doi.org/10.1016/j.proci.2016.06.003
1540-7489

pollutant abatement in natural-gas-driven vehicles [3]. In large-scale power generation, catalytic processes appear particularly attractive for the latest combustion technologies aiming at mitigating greenhouse CO_2 emissions. Post-combustion capture of CO_2 in natural-gas-fired gas turbines can be accomplished by employing flue gas recirculation (FGR) in the reactant stream, which increases the CO_2 content in the exhaust gas and thus facilitates its subsequent capture [4]. The reduced reactivity of the FGR-diluted natural gas favors the use of catalytic combustion methodologies due to their lower effective activation energy.

Supported palladium and platinum catalysts are preferred due to their highest activity towards methane total oxidation. Nonetheless, rhodium-based catalysts used as promoters or additives in other noble metals, have also received increased attention despite their lower activity. Addition of Rh into Pt has shown to improve (under certain Rh/Pt compositions) the Pt activity towards methane total oxidation [5], while addition of Rh on Pd can improve the long-term stability of Pd without crucially affecting its activity [6,7]. Furthermore, it has been suggested that the apparent lower activity of Rh compared to Pd and Pt in technical catalysts may be a result of Rh/support interactions under strong oxidizing conditions at high temperatures [8].

The total oxidation of methane under elevated pressures relevant to power generation has been investigated mostly over Pt and Pd catalysts [9–12]. In fuel-lean CH_4/air combustion over Pt at pressures up to 14 bar, Reinke et al. [9] applied in situ spatially-resolved Raman measurements and derived a pressure dependence $\sim p^{0.47}$ for the methane catalytic reactivity. For Pd catalysts key issue has been the decomposition temperature of the active PdO phase to the less active Pd [11] (it increased from ~790 to ~980 K as pressure increased from 1 to 16 bar). On the other hand, high-pressure studies for methane oxidation over Rh were mainly performed at fuel-rich stoichiometries due to the importance of this catalyst for methane catalytic partial oxidation, which is in turn used for syngas production and synthesis of liquid fuels at elevated pressures [13,14]. Under fuel-lean conditions, there are overall fewer studies [15,16] and this is exacerbated at high pressures. Deshmukh and Vlachos [16] studied fuel-lean CH_4/air combustion over Rh and developed surface reaction mechanisms validated at atmospheric pressure.

The present work investigates the hetero-/homogeneous combustion of fuel-lean $CH_4/O_2/N_2$ mixtures over Rh at pressures 2–12 bar. In situ Raman measurements of major gas-phase species concentrations and planar laser induced fluorescence (LIF) of the OH radical were performed in an optically accessible channel-flow reactor coated with Rh, while 2-D simulations were carried out

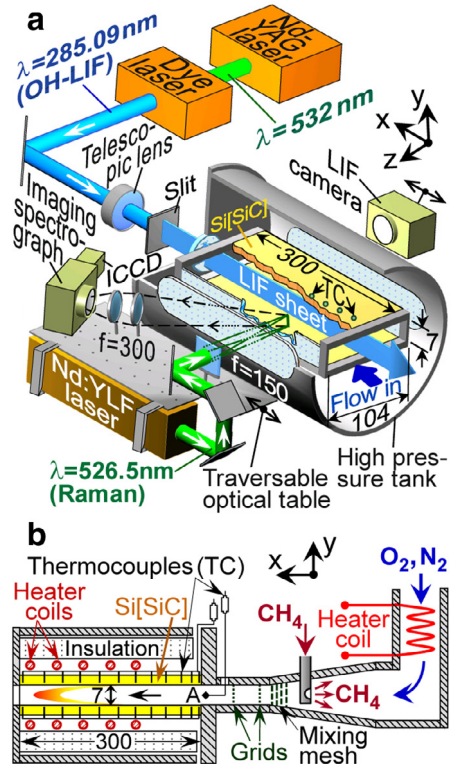

Fig. 1. (a) Test rig and Raman/LIF setup, (b) reactor details. All distances are in mm.

with detailed hetero-/homogeneous chemical reaction schemes. Goals were to determine the pressure dependence for the methane reactivity, assess the applicability of various hetero-/homogeneous reaction schemes, and investigate the conditions leading to homogeneous ignition.

2. Experimental

2.1. High-pressure catalytic reactor

The channel reactor comprised two horizontal Si[SiC] ceramic plates (300 mm long ($-x$), 104 mm wide ($-z$), 9 mm thick, positioned 7 mm apart ($-y$)) and two 3-mm-thick vertical quartz windows (see Fig. 1 and further [17,18]). The inner Si[SiC] surfaces were coated with Rh using plasma vapor deposition (PVD). A 1.5-μm-thick non-porous Al_2O_3 layer was first deposited on the Si[SiC] and then a 2.2-μm-thick Rh layer on top of the Al_2O_3. The appreciably thick 2.2 μm noble metal layer closely resembled a polycrystalline surface and this was verified with total and active surface area measurements using BET (Kr-physisorption) and CO-chemisorption, respectively, which confirmed the lack of surface porosity.

Temperatures were measured by S-type thermocouples (12 for each plate, positioned along the x–y symmetry plane, see Fig. 1), whose beads were embedded 0.9 mm beneath the catalyst surfaces by eroding 8.1-mm-deep and 1.2-mm-diameter holes from the rear uncoated Si[SiC] sides. Over the length $100 < x < 300$ mm, two resistive coils with adjustable power were positioned above the Si[SiC] plates to counteract external heat losses and to regulate the surface temperatures (Fig. 1b). The reactor was mounted inside a 1.8-m-long high-pressure cylindrical steel tank. Two 350-mm-long, 50-mm-high and 35-mm-thick quartz windows on the tank sides provided optical accessibility in the lateral ($-z$) direction (Fig. 1a). Two quartz windows at the rear tank flange and the reactor exhaust allowed for an additional streamwise ($-x$) optical access.

CH_4 (99.95% purity), O_2, and N_2 were supplied by pressurized bottles and their flows were controlled by three Brooks flowmeters. O_2 and N_2 were mixed in two sequential static mixers and then preheated electrically (Fig. 1b). Methane was injected counterflow to the preheated O_2/N_2 stream inside a 200-mm-long steel conical section (specifically designed to mitigate autoignition of the preheated and pressurized $CH_4/O_2/N_2$ mixture) by means of eight 0.5-mm-diameter nozzles arranged in the z-direction (Fig. 1b). The conical section gradually adjusted the cross sectional area from circular (35-mm-diameter) to the final rectangular channel shape ($104 \times 7\ mm^2$). A 3-mm-thick wire mesh and two fine grids ($0.5\ mm^2$ open area) inside the conical section yielded good mixing of the methane with O_2/N_2 and a uniform outlet velocity. Optimization of the number and axial positions of the mesh/grids was accomplished by the following room-temperature measurements performed at the exit plane of the stand-alone conical section: hot wire velocimetry to assess the flow uniformity, and planar LIF of NO (doped into the CH_4 stream, excitation at 226.25 nm and detection at 240–265 nm) to assess the mixing quality. The gas temperature at the reactor inlet ($x = 0$, location A in Fig. 1b) was measured by a K-type thermocouple, whose bead was radiation-shielded by encapsulating it inside a 1.2 mm-ID and 2.0 mm-OD ceramic tube.

2.2. Laser diagnostics

The Raman and OH-LIF setups are illustrated in Fig. 1a. For Raman, a frequency-doubled pulsed Nd:YLF laser (Quantronix Darwin-Duo, repetition frequency 2 kHz) provided a radiation at 526.5 nm, with a pulse duration and energy of 120 ns and 40 mJ, respectively (Fig. 1a). An $f = 150$ mm cylindrical lens focused the laser beam into a ~0.3 mm thick vertical line that spanned the 7 mm channel height and was offset laterally ($z = 15$ mm) to increase the collection angle and minimize thermal beam steering, as in earlier studies [17,18]. Two $f = 300$ mm lenses focused the Raman-scattered light into the entrance slit of a 25 cm spectrograph (Chromex-250i) equipped with an intensified CCD camera (Princeton Instruments PI-MAX1024GIII, 640×255 pixels corresponding to spectral shift and transverse distance, respectively). Excitation radiation was suppressed by an appropriately tilted Kaiser optical systems 532 nm holographic notch filter and a selected OG550 Schott colored glass filter.

The Nd:YLF laser, the sending/collecting optics and the spectrograph were mounted on a traversable optical table (Fig. 1a), allowing measurements over $9 \le x \le 126$ mm. To increase the signal-to-noise ratio, Raman-scattered light from typically 300,000 laser pulses was integrated on the detector chip. The 7 mm channel-height was recorded on 220 pixels, which were subsequently binned to 64 pixels. The effective Raman cross-sections, which included transmission efficiencies (windows, lenses, filter, spectrometer and camera), were evaluated by recording the signals of several pressurized CH_4, N_2 and CO_2 containing mixtures, air, and the actual feed mixture. The procedure for assessing the Raman data has been elaborated in our previous work [9]. The measurement accuracy was ± 3% for species concentrations ≥ 3% vol. and ± 8% for concentrations as low as 0.5% vol., while lower compositions could not be accurately resolved. Due to low signal-to-noise ratios, Raman data-points closer than 0.7 mm to both catalytic walls were discarded.

For OH-LIF, the 532 nm s harmonic of a pulsed Nd:YAG laser (Quantel YG781C20 CL-D-LNE3, pulse duration 10 ns and repetition rate 20 Hz) pumped a Quantel TDL90-NBP2EWT UVT3 dye laser (the dye was 90% Rhodamine 6 G and 10% Rhodamine B in ethanol). The output radiation was frequency-doubled to generate the 285.09 nm excitation beam with pulse energy of 8 mJ. A telescopic lens and a slit transformed the 285.09 nm beam into a vertical light sheet that propagated counterflow along the reactor's x–y symmetry plane (Fig. 1a). Using the central 50% of the beam and by a mild focusing, the signal was optimized without saturating the $P_1(7)$ $A(v' = 1) \leftarrow X(v'' = 0)$ OH transition. An intensified CCD camera (LaVision Imager Compact HiRes-IRO, 1392×1024 pixels binned to 696×512) recorded the OH fluorescence at 90° through the reactor and tank side-windows. Fluorescence was collected by an EADS Sodern CERCO®-2178 f100 mm/2.8 UV antireflection-coated lens from both (1–1) and (0–0) transitions at 308 and 314 nm, respectively, using a BK-310-11 bandpass interference filter. Channel areas $100 \times 7\ mm^2$ were recorded on 1360×70 pixels of the CCD chip. To map the entire reactor length, the camera was traversed axially in steps

of 50 mm. At each position 400 images were integrated to increase the signal-to-noise ratio.

3. Numerical

Simulations were performed with a full-elliptic 2-D steady CFD code (details in [17,18]). A staggered grid with 460 × 64 points (in x- and y-, respectively) for the 300 × 7 mm^2 channel domain was sufficient to produce a grid independent solution. Temperature profiles at the lower ($y = 0$) and upper ($y = 7$ mm) channel walls were constructed by fitting curves through the 12 thermocouple measurements on each Si[SiC] plate, and then imposed as boundary conditions in the simulations. The temperature, axial velocity and species mass fractions were uniform at the inlet (assessed by the inlet thermocouple and the flowmeters).

For the oxidation of methane on Rh, the latest detailed reaction mechanism by Deutschmann (Karakaya et al. [19]) was used (13 surface and 6 gaseous species, 48 reactions), with a surface site density of 2.7 × 10^{-9} mol/cm^2. This mechanism has been tested for methane oxidation and reforming in annular-flow and stagnation-flow reactors at atmospheric pressure. Additionally, a reduced mechanism from Deshmukh and Vlachos [16] (10 surface and 4 gaseous species, 15 reactions) was investigated. For gas-phase chemistry of fuel-lean CH_4/air mixtures, three elementary C_1/H/O mechanisms were examined, which also included the part of C_2 chemistry that led to recombination of C_1 radicals to C_2 species: Warnatz et al. [20] (25 species, 108 reactions including appropriate pressure dependencies for the reactions $CH_3+H \Leftrightarrow CH_4$, $CH_3+CH_3 \Leftrightarrow C_2H_6$, $CH_3OH \Leftrightarrow CH_3+OH$), GRI-3.0 [21] (26 species, 137 reactions) and Leeds [22] (25 species, 105 reactions). Although the Warnatz [20] mechanism had reproduced homogeneous ignition in earlier studies of fuel-lean CH_4/air combustion over Pt [4,23], the considerably lower temperatures in the current experiments necessitated the investigation of additional mechanisms.

Surface and gas-phase chemical reaction rates were evaluated with Surface-Chemkin [24] and Chemkin [25], respectively. Mixture-average diffusion including thermal diffusion was used in conjunction with the Chemkin transport database [26].

4. Results and discussion

Pressures 2–12 bar and equivalence ratios $\varphi = 0.30$–0.40 were investigated (see Table 1). The catalytic reactivity was assessed with the Raman measurements, while OH-LIF was applied for selected cases to investigate homogeneous combustion. In all cases where Raman measurements were used to assess the catalytic reactivity, OH-LIF was still applied to ensure the absence of homogeneous combustion within the axial extent of the Raman measurements (a necessary step to avoid falsification of the catalytic kinetics by gaseous chemistry). Cases with OH-LIF measurements generally had higher inlet temperatures (see Table 1) in order to facilitate homogeneous ignition. The flows were laminar with inlet Reynolds numbers (based on the channel height) 470–750. Before each test, the catalyst was reduced in a H_2/N_2 flow at 920 K for 30 min.

Table 1
Experimental conditions[a].

Case	p	φ	U_{IN}	T_{IN}	CH_4	O_2
1^R	2	0.30	1.25	395	4.4	29.7
2^R	2	0.38	1.26	392	5.4	28.6
3^R	5	0.33	0.41	437	4.8	29.2
4^R	5	0.40	0.50	387	5.5	27.5
$5^{R,L}$	8	0.32	0.30	425	4.7	29.6
6^R	8	0.40	0.32	386	5.5	27.5
7^R	10	0.35	0.25	386	5.2	29.5
8^R	10	0.40	0.26	384	5.5	27.5
9^R	12	0.35	0.21	377	5.2	29.3
10^R	12	0.38	0.21	382	5.5	28.8
11^L	2	0.38	1.25	461	5.5	29.0
12^L	5	0.33	0.53	476	4.8	29.2
13^L	10	0.35	0.24	439	5.1	28.8
14^L	12	0.40	0.21	440	5.2	26.2

[a] Pressure (bar), equivalence ratio, inlet velocity (m/s), inlet temperature (K), CH_4 and O_2 vol. content (%), balance N_2.
[R] Cases with Raman.
[L] Cases with OH-LIF.

4.1. Catalytic reactivity

Comparisons between measured and predicted (using the kinetic scheme from Deutschmann [19]) transverse profiles of the limiting methane reactant are illustrated in Figs. 2 and 3. For clarity, up to 18 of the total 64 transverse data points are shown, spanning the experimentally-resolvable height 0.7 mm ≤ y ≤ 6.3 mm. The computed transport-limited (i.e. infinitely-fast chemistry) solutions for the last axial positions are also plotted in Figs. 2 and 3 (marked as TL). The TL profiles have zero methane concentration at both walls ($y = 0$ and 7 mm) and provide physical lower limits for the methane mole fractions in Figs. 2 and 3. The operating conditions in Table 1 have been selected to fall in the kinetically-controlled regime, far away from the transport limit (i.e. methane mole fractions well-above zero at the walls), which was a cardinal requirement for assessing the catalytic reactivity.

For the lowest pressure of 2 bar (Fig. 2(1,2)), the scheme from Deutschmann [19] reproduced the near-wall bending of the methane profiles at all axial positions; this was evident despite the lack of

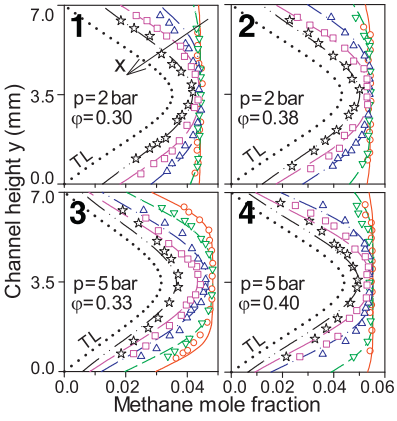

Fig. 2. Comparisons of Raman-measured (symbols) and predicted (lines, using the kinetic scheme from [19]) transverse profiles of methane mole fractions for Cases 1–4; $x=9$ mm (circles, solid lines), 21 mm (lower triangles, short-dashed lines), 51 mm (upper triangles, dashed-dotted lines), 80 mm (squares, long-dashed lines) and 126 mm (stars, dashed-double-dotted lines). Dotted lines marked TL are transport-limited predictions at $x=126$ mm.

Raman data closer than 0.7 mm from both walls. Predictions with the reduced fuel-lean methane 15-step-mechanism from [16] are shown for Case 2 in Fig. 4. While at $x=9$ and 21 mm there was a good agreement with the measurements (see Fig. 4(a)), predictions farther downstream gave much higher reactivity (Fig. 4(b)); in particular, the predictions at $x=80$ mm (long-dashed lines) and $x=126$ mm (dashed-doubled-dotted line) reached transport limited methane conversions. It is noted that the TL solution at $x=126$ mm in Fig. 4(b) (dotted line) still differed from the kinetic prediction at the same axial position (dashed-double-dotted line) as the former referred to a transport limited conversion already from the beginning of the channel. The discrepancies in Fig. 4(b) were not surprising as the reaction scheme in [16] was developed for low temperatures, validated against the atmospheric-pressure data from Burch et al. [15] at temperatures up to 775 K. However, the upper and lower wall temperature profiles for Case 2 (see Fig. 5(a)) were above 800 K for $x \geq 9$ mm. Moreover, for most cases with Raman measurements the wall temperatures typically exceeded 775 K already at the first measuring location $x=9$ mm (see Fig. 5). For this reason, all subsequent simulations were performed with the Deutschmann mechanism.

At 5 bar the deviations between measurements and predictions became noticeable, as seen at the last two axial locations in Fig. 2(3,4) where the catalytic reactivity was overpredicted. The overprediction of catalytic reactivity at the downstream axial locations (wherein the wall temperature was higher) was further accentuated at the pressures 8–12 bar. This was evident at the last two axial locations in

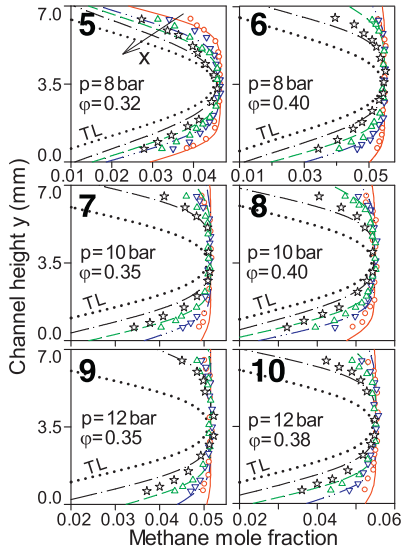

Fig. 3. Comparisons between measured (symbols) and predicted (lines, using the kinetic scheme from [19]) transverse profiles of methane mole fractions for Cases 5–10; $x=9$ mm (circles, solid lines), 21 mm (lower triangles, dashed-double-dotted lines), 31 mm (upper triangles, dashed lines) and 51 mm (stars, dashed-dotted lines). Dotted lines marked TL are transport-limited predictions at $x=51$ mm.

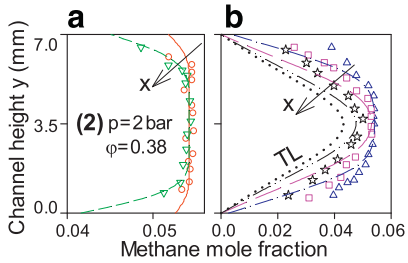

Fig. 4. Comparisons between measured (symbols) and predicted (lines, using the kinetic scheme from [16]) transverse profiles of methane mole fractions for Case 2. The notation of axial locations for the predictions and measurements is the same as in Fig. 2. Dotted line marked TL in (b) is the transport-limited prediction at $x=126$ mm.

Fig. 3 where the measured methane mole fractions (stars and upper triangles) were appreciably higher than the predictions at the same y-position (see, for example, the region $y<3$ mm in Fig. 3). Our previous investigation of fuel-lean methane/air catalytic combustion over platinum [9] had shown that key to the high-pressure aptness of a catalytic mechanism was its ability to capture the reduction in surface free-site coverage (and the corresponding increase in oxygen coverage) with increasing pressure. This in turn restrained the rate of increase of the catalytic reactivity with rising pressure. A single-step for lean methane combustion, first-order with

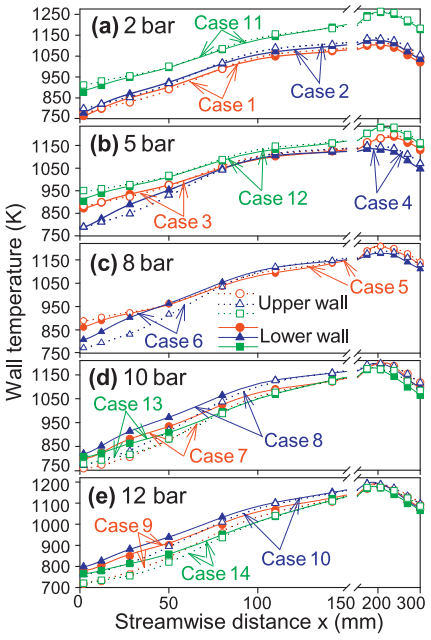

Fig. 5. Measured upper-wall and lower-wall temperatures for all cases.

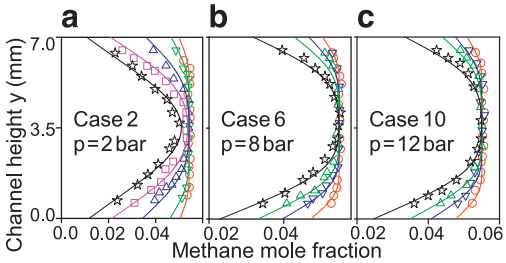

Fig. 6. Measured (symbols) and predicted (lines, global step of Eq. (1)) methane mole fractions. Symbol notations are as in Fig. 2 (Case 2) and Fig. 3 (Cases 6 and 10).

respect to methane and zero with respect to oxygen, was proposed in [9] for pressures up to 16 bar:

$$\dot{s}_{CH_4} = A(p/p_o)^{-n}\exp(-E_a/RT)[\mathrm{CH_4}], \qquad (1)$$

where for platinum the (negative) pressure exponent was $n=0.53$. This negative power law slowed down the increase in catalytic reactivity with rising pressure, such that $\dot{s}_{CH4}\sim p^{1-n}$ (when also considering the linear pressure dependence of the concentration $[CH_4]$ in Eq. (1)). For rhodium, the step of Eq. (1) was also adopted, with the following fitted kinetic parameters: $A=1.6\times10^5$ cm/s, apparent activation energy $E_a=85$ kJ/mol, $n=0.70$ and $p_o=2$ bar. Predictions with this global step were in quite good agreement with the measurements over the entire range 2 bar $\le p \le$ 12 bar, as shown in Fig. 6. Thus, the methane reactivity on rhodium exhibited an overall pressure dependence

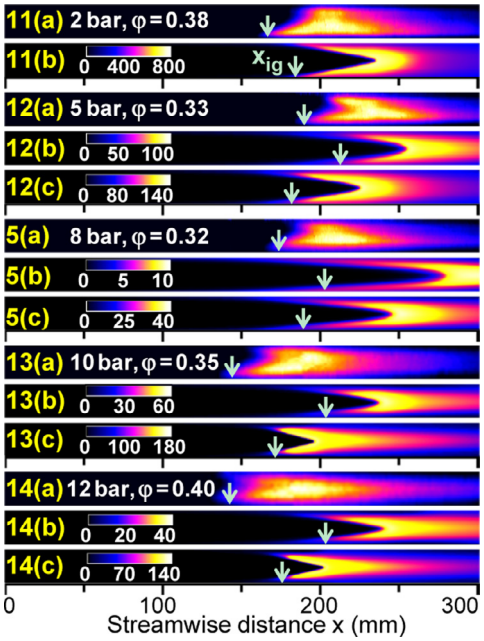

Fig. 7. Two-dimensional OH distributions for five cases: (a) OH-LIF, (b) predictions with the catalytic scheme from [19] and the Leeds gaseous mechanism, (c) predictions with the one-step catalytic reaction from Eq. (1) and the Leeds mechanism. Color-coded bars provide predicted OH (ppmv).

$1-n=0.30$, which was weaker than that of platinum ($=0.47$). This was an outcome of the relative adsorption/desorption strengths of methane and oxygen on the particular noble metal.

The measured wall temperatures in Fig. 5 were a result of reaction exothermicity and heat input from the heater coils discussed in Section 2.1. By decreasing the power of the heater coils with rising pressure, the increased catalytic reactivity at higher pressures could be restrained such that kinetically controlled conversion could always be attained over a wide pressure range (see Figs. 2 and 3). Finally, the methane catalytic conversions at the channel exit predicted with the one-step scheme in Eq. (1) ranged from 49% (Case 1) to 80% (Case 4).

4.2. Homogeneous combustion

Comparisons between measured and predicted OH distributions are shown in Fig. 7 for the five cases in Table 1 with LIF measurements. Vertical arrows indicate the onset of homogeneous ignition (x_{ig}), defined as the far-upstream position where OH reached 5% of its peak predicted or measured value in the channel. All simulations in Fig. 7 referred to the Leeds gas-phase mechanism [22]. For surface chemistry the Deutschmann [19] surface mechanism was used; moreover,

simulations with the global catalytic step of Eq. (1) are shown for cases with $p \geq 5$. The other two investigated gas-phase mechanisms (Warnatz [20] and GRI-3.0 [21]) failed to yield homogeneous ignition for all examined cases. At 2 bar the agreement between measurement (Fig. 7(11a)) and simulation (Fig. 7(11b)) was good in terms of homogeneous ignition position and flame length. For the cases with $p \geq 5$ the Leeds mechanism together with the Deutschmann mechanism always overpredicted the homogeneous ignition distance, with the overprediction increasing with rising pressure. Characteristically, while the OH-LIF at 5 bar yielded $x_{ig} = 190$ mm (Fig. 7(12a)) and the simulation $x_{ig} = 212$ mm (Fig. 7(12b)), the corresponding OH-LIF and prediction at 12 bar were $x_{ig} = 141$ mm (Fig. 7(14a)) and $x_{ig} = 205$ mm (Fig. 7(14b)). The overpredictions at $p \geq 5$ bar, largely reflected the faster catalytic consumption of methane with the employed heterogeneous scheme [19] (discussed in the previous section), which in turn reduced the amount of methane available for gaseous combustion. Using the global catalytic step from Eq. (1) and the Leeds gaseous mechanism, the predicted flame positions approached the measurements ($x_{ig} = 183$ mm in Fig. 7(12c) and $x_{ig} = 175$ mm in Fig. 7(14c)).

While the Warnatz mechanism [20] (with an improved rate for the branching step CHO+M⇔CO+H+M) had reproduced the onset of homogeneous ignition in earlier studies of fuel-lean methane combustion over platinum at pressures up to 16 bar [23], it could not capture homogeneous ignition in this work. This was due to the substantially lower temperatures in the present rhodium experiments. In the earlier Pt studies, the inlet temperatures were 560–754 K (as opposed to the herein 425–476 K, see Table 1) while the wall temperatures over the gaseous induction zones were 1100–1350 K (as opposed to typically 700–1150 K in the present work, see Fig. 5). Catalytic combustion at such ultra-lean stoichiometries and preheats have not been elaborated in the literature. Moreover, the actual stoichiometry at homogeneous ignition was appreciably reduced from the already low inlet values of Table 1 due to the upstream catalytic conversion. This resulted in predicted (using the Deutschmann/Leeds mechanisms) effective CH_4/O_2 equivalence ratios 0.17–0.29 at the homogeneous ignition locations of the cases in Fig. 7.

The origin of the differences among the three gas-phase mechanisms was further studied by computing ignition delay times of CH_4/air mixtures with equivalence ratios 0.15–0.40, pressures of 2 and 12 bar and constant temperatures of 900 and 1300 K. The fixed temperatures mimicked the hot walls in the channel-reactor of Fig. 1, which were primarily established by the catalytic reaction pathway. The ignition delays in Fig. 8 (computed using the SENKIN package of Chemkin [27]) were defined as the times at which the methane concentrations dropped to 50% of their initial values.

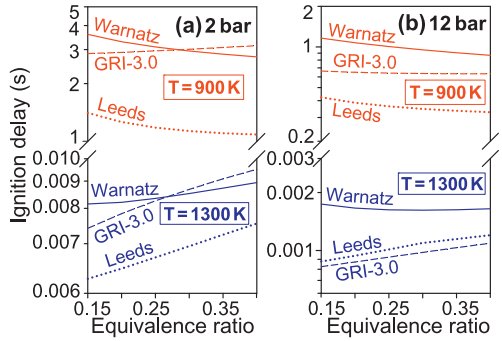

Fig. 8. Ignition delays of CH_4/air mixtures as a function of equivalence ratio for two pressures, two temperatures and three gas-phase reaction mechanisms.

The lower temperature 900 K was particularly relevant for cases with $p \geq 5$ bar in Fig. 7, whereby the wall temperatures ranged from ~700 K to ~1150 K over the gaseous induction zones $x < x_{ig}$ (see Fig. 5). The 1300 K referred to the hottest wall temperature profiles of the earlier platinum studies [23]. While at 1300 K the ignition delays deduced from the Leeds mechanism were by a factor of at most ~1.8 shorter than those of Warnatz, this factor increased to ~2.8 at 900 K (Fig. 8), thus rendering the Leeds mechanism considerably more reactive at lower temperatures. Sensitivity analysis indicated that although many reactions contributed to the aforementioned differences, the reaction $CH_3+HO_2 \Leftrightarrow CH_4+O_2$ (whose net rate was positive in the induction zone close to ignition) was slower in the Leeds mechanism and accounted for up to 30% of the computed differences in ignition delays among the three mechanisms. Hence, at the present low temperatures Leeds was shown to be an appropriate reaction mechanism. Finally, for the current very lean stoichiometries, the self-inhibition of methane (ignition delays increasing with rising equivalence ratios, as reported in [28] but for higher $\varphi > 0.40$) was not always observed in Fig. 8.

5. Conclusions

The catalytic and gas-phase combustion of fuel-lean $CH_4/O_2/N_2$ mixtures was investigated experimentally and numerically at pressures 2–12 bar in a 7-mm-height, Rh-coated catalytic channel. Simulations were performed with a 2-D elliptic code, which included detailed heterogeneous and homogeneous chemical reaction mechanisms. Comparisons between Raman-measured and numerically-predicted transverse profiles of

methane mole fractions have led to the evaluation of the performance of detailed surface reaction mechanisms and to the construction of an appropriate one-step catalytic reaction. It was shown that for the investigated pressures, the catalytic reactivity of methane over rhodium exhibited a pressure dependence $\sim p^{0.30}$, which was weaker than the $\sim p^{0.47}$ dependence reported earlier for methane oxidation over platinum.

Gas-phase combustion was investigated with planar OH-LIF. The LIF measurements exemplified the importance of the low equivalence ratios and modest temperatures in the predictive capacity of various gas-phase chemical reaction mechanisms. The Leeds gas-phase mechanism was shown to reproduce the onset of homogeneous ignition at pressures 2–12 bar, particularly when used in conjunction with the aforementioned one-step catalytic reaction.

Acknowledgments

Support was provided by the project EU-HRC. We thank Prof. Olaf Deutschmann for providing his latest surface mechanism and Mr. Jürgen Theile for aiding the measurements.

References

[1] R. Carroni, T. Griffin, J. Mantzaras, M. Reinke, *Catal. Today* 83 (2003) 157–170.
[2] N.S. Kaisare, D.G. Vlachos, *Prog. Energy Combust. Sci.* 38 (2012) 321–359.
[3] D. Bounechada, G. Groppi, P. Forzatti, K. Kallinen, T. Kinnunen, *Appl. Catal. B Environ.* 119 (2012) 91–99.
[4] M. Reinke, J. Mantzaras, R. Schaeren, R. Bombach, A. Inauen, S. Schenker, *Proc. Combust. Inst.* 30 (2005) 2519–2527.
[5] M. Bhagiyalakshmi, R. Anuradha, S.D. Park, T.S. Park, W.S. Cha, H.T. Jang, *Bull. Korean Chem. Soc.* 31 (2010) 120–124.
[6] A. Maione, F. Andre, P. Ruiz, *Appl. Catal. A Gen.* 333 (2007) 1–10.
[7] C.K. Ryu, M.W. Ryoo, I.S. Ryu, S.K. Kang, *Catal. Today* 47 (1999) 141–147.
[8] R. Burch, D.J. Crittle, M.J. Hayes, *Catal. Today* 47 (1999) 229–234.
[9] M. Reinke, J. Mantzaras, R. Schaeren, R. Bombach, A. Inauen, S. Schenker, *Combust. Flame* 136 (2004) 217–240.
[10] M. Reinke, J. Mantzaras, R. Bombach, S. Schenker, N. Tylli, K. Boulouchos, *Combust. Sci. Technol.* 179 (2007) 553–600.
[11] D. Ciuparu, M.R. Lyubovsky, E. Altman, L.D. Pfefferle, A. Datye, *Catal. Rev. Sci. Eng.* 44 (2002) 593–649.
[12] H. Yamamoto, H. Uchida, *Catal. Today* 45 (1998) 147–151.
[13] A. Bitsch-Larsen, R. Horn, L.D. Schmidt, *Appl. Catal. A Gen.* 348 (2008) 165–172.
[14] A. Schneider, J. Mantzaras, R. Bombach, S. Schenker, N. Tylli, P. Jansohn, *Proc. Combust. Inst.* 31 (2007) 1973–1981.
[15] R. Burch, P.K. Loader, N.A. Cruise, *Appl. Catal. A Gen.* 147 (1996) 375–394.
[16] S.R. Deshmukh, D.G. Vlachos, *Combust. Flame* 149 (2007) 366–383.
[17] Y. Ghermay, J. Mantzaras, R. Bombach, K. Boulouchos, *Combust. Flame* 158 (2011) 1491–1506.
[18] X. Zheng, J. Mantzaras, R. Bombach, *Combust. Flame* 160 (2013) 155–169.
[19] C. Karakaya, L. Maier, O. Deutschmann, *Int. J. Chem. Kinet.* 48 (2016) 144–160.
[20] J. Warnatz, R.W. Dibble, U. Maas, Combustion, *Physical and Chemical Fundamentals, Modeling and Simulation*, Springer-Verlag, New York, 1996.
[21] G.P. Smith, D.M. Golden, M. Frenklach, et al., GRI 3.0 Mechanism, available at: www.me.berkeley.edu/gri_mech/, 1999.
[22] K.J. Hughes, T. Turøanyi, A. Clague, M.J. Pilling, *Int. J. Chem. Kinet.* 33 (2001) 513–538.
[23] M. Reinke, J. Mantzaras, R. Bombach, S. Schenker, A. Inauen, *Combust. Flame* 141 (2005) 448–468.
[24] M.E. Coltrin, R.J. Kee, F.M. Rupley, *Surface Chemkin: A Fortran Package for Analyzing Heterogeneous Chemical Kinetics at the Solid Surface–Gas Phase Interface*, Report No. SAND90-8003C, Sandia National Laboratories, 1996.
[25] R.J. Kee, F.M. Rupley, J.A. Miller, *Chemkin II: A Fortran Chemical Kinetics Package for the Analysis of Gas-Phase Chemical Kinetics*, Report No. SAND89-8009B, Sandia National Laboratories, 1996.
[26] R.J. Kee, G. Dixon-Lewis, J. Warnatz, M.E. Coltrin, J.A. Miller, *A Fortran Computer Code Package for the Evaluation of Gas-Phase Multicomponent Transport Properties*, Report No. SAND86-8246, Sandia National Laboratories, 1996.
[27] A.E. Lutz, R.J. Kee, J.A. Miller SENKIN, *A Fortran Program for Predicting Homogeneous Gas-Phase Chemical Kinetics with Sensitivity Analysis* (1996) Report No. SAND87-8248.
[28] L.J. Spadaccini, M.B. Colket, *Prog. Energy Combust. Sci.* 20 (1994) 431–460.